ANALYSIS OF BRDF CHARACTERISTICS OF FOREST STANDS WITH A DIGITAL AERIAL FRAME CAMERA

T. Koukal [a, *], W. Schneider [a]

[a] Institute of Surveying, Remote Sensing and Land Information, University of Natural Resources and Applied Life Sciences, Vienna, Austria
(tatjana.koukal, werner.schneider@boku.ac.at)

KEY WORDS: Digital, Aerial, Photography, Land Cover, Forestry, Radiometry, Analysis, Modelling

ABSTRACT:

The directional reflectance characteristics of the land surface can be described based on concepts of the Bidirectional Reflectance Distribution Function (BRDF). This contribution concentrates on directional reflectance effects in aerial photos of forests. Since the advent of digital metric aerial photography, major efforts have been made to apply quantitative digital automatic methods for the analysis of aerial photos. Directional reflectance effects are important for this: on the one hand, they make analysis more complicated, on the other hand they may provide additional information for deducing land cover (e.g. forest) parameters. Digital aerial photos, when taken with high forward and side overlap, may provide a convenient tool for analysing directional reflectance effects. The main aim of this contribution is to demonstrate the usefulness of digital aerial photos taken with a Vexcel UltraCamD for analysing directional reflectance characteristics of forests. 11 BRDF models are tested for 6 different land cover types focusing on forest cover. The models were evaluated using the coefficient of determination (R^2) and the symmetric mean absolute percentage error (sMAPE). It has been shown that the parameters of BRDF models describing individual forest plots can be estimated from digital aerial photos taken with a frame camera with large forward and side overlap. Differences in the performance of the models for different forest plots could be explained taking into account the special assumptions on which the models are based and the special properties of the observed forest stands.

1. INTRODUCTION

In the analysis of remotely sensed images, information on land cover is mainly deduced from the reflectance properties of the terrain surface. Reflectance is a function of wavelength and of irradiation and observation directions. These directional reflectance characteristics can be described based on concepts of the Bidirectional Reflectance Distribution Function (BRDF) (Schaepman-Strub et al., 2006).

While BRDF aspects often can be neglected in the analysis of satellite images sensed with vertical view direction and with a small angular field of view (e.g. of Landsat images), the directional reflectance properties are important for image data from sensors with steerable view direction (e.g. Ikonos) and from sensors with a large angular field of view (e.g. MODIS, or aerial scanners and aerial cameras). BRDF effects are particularly noticeable in the case of surfaces of a pronounced vertical structure, e.g. forest canopies.

This contribution concentrates on the directional reflectance effects in aerial photos of forests. A quantitative treatment of this subject is of interest for the following reasons:

(1) In the past, aerial photos were recorded in analogue form on photographic film. They were of poor radiometric quality. Digital automatic image analysis therefore did not seem very promising and was hardly applied operationally for the evaluation of aerial photos. Rather, the usage of aerial photos (e.g. in forestry) primarily relied on labour-intensive and subjective visual interpretation. It is only now, after the advent of digital metric aerial photography, that major efforts are made to apply quantitative digital automatic methods also for the analysis of aerial photos. The BRDF-related effects (including the well-known hot spot phenomenon) in aerial photos which are usually taken with a large angular field of view pose a major challenge in this undertaking. These effects on the one hand make analysis more complicated, on the other hand they may provide additional information for deducing land cover (e.g. forest) parameters. It is desirable to expand the knowledge in this field.

(2) Directional reflectance data on different types of land-cover usually are obtained by measurements either in the laboratory on small samples or in the field by employing special platforms and constructions. It is impossible to perform directional measurements on forest canopies in the lab, and it is very difficult to implement outdoor directional reflectance measurements on timber trees and old stands. However, digital aerial photos, when taken with high forward and side overlap, provide a convenient tool for analysing directional reflectance effects. It is an additional special advantage of using aerial photography that analysis may be performed at different scales: Working with full resolution of the aerial photos (e.g. pixel sizes of 20 cm to 100 cm), one may study directional reflectance at individual trees and parts of trees (sunlit branches, treetops, etc.). When using reduced resolution (by averaging over pixel windows of the order of 20 m x 20 m or 50 m x 50 m), directional reflectance characteristics including the shadow effects of forest canopies due to crown shape, crown closure and ground vegetation may be analysed. On the other hand, a limitation of aerial photography is given by the restriction to (usually) 4 spectral bands in the visible and near infrared parts of the spectrum.

The main aim of this contribution is to demonstrate the usefulness of digital aerial photography with frame cameras for analysing BRDF-related characteristics of forests. In particular, a number of BRDF models are tested for their usefulness to describe the directional patterns of pixel values as obtained with a Vexcel UltraCam aerial frame camera. The directional reflectance functions obtained can be considered as

* Corresponding author

approximations to BRDF only, as the hemispherical irradiance component (diffuse sky radiation) is present in addition to the directional irradiation from the sun.
Large windows of pixels are used, causing the directional reflectance functions to include shadow effects due to crown shape, crown density etc.

2. METHOD

Basically there are two possibilities to employ wide-angular-view-sensors for studying directional reflectance effects: Single images may be used, if large homogeneous stands covering the entire area of an image are available. In this case, a sample of plots distributed over one image (and therefore viewed from different directions) is analysed, and the BRDF model parameters are deduced from the pixel values of this sample (Dymond and Trotter, 1997). Alternatively, if images with sufficient forward and side overlap are available, the same plot on the ground is viewed from different directions on different images. In this second case, the BRDF model parameters of every single terrain element may be derived. No assumptions on the homogeneity of stands beyond the area of an individual plot are required. This second approach was chosen for the work described here.
There are two different types of digital camera systems available: line cameras (e.g. ADS40 by Leica Geosystems) and frame cameras (e.g. DMC by Intergraph/ZI-Imaging, UltraCamX by Vexcel Imaging). In BRDF analysis, the number of different directions of view on a terrain element that can be obtained at one overflight is decisive. In case of a line scanner, this number is determined by the number of CCD lines in the focal plane. E.g. the ADS40 camera is a 3-line-camera leading to 3 different directions of view per terrain element and overflight. In case of a frame camera, the number of directions of view is dependent on the percentage of forward overlap. Digital frame cameras achieve forward overlaps of 90 % and higher and, as a consequence, 10 directions of view and more.
The number of viewing directions also increases with the overlap between the flight lines (side overlap). E.g. in a mission with 90 % forward overlap and 30 % side overlap, any terrain element is observed from 10 to 20 view directions depending on the object's position within the path (Figure 1).

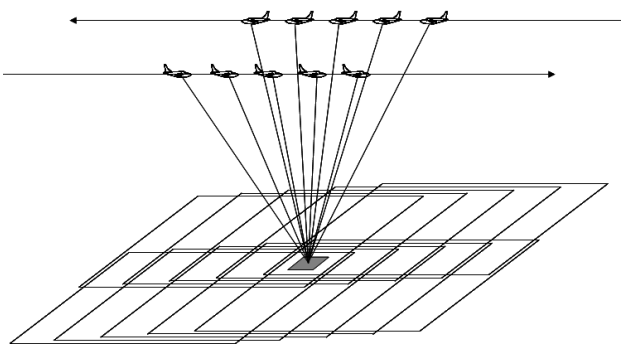

Figure 1. Directions of view on a terrain element in aerial photography with forward and side overlap

Another key parameter for BRDF-related investigations is the angular field of view (FOV) both along and across the track as it defines the range of viewing angles (from vertical) at which the terrain elements can be observed.

In this study, images taken with the digital metric camera Vexcel UltraCamD were used. Relevant parameters of camera and images are listed in chapter 4.
While the input data (pixel values) for many BRDF models may be given in arbitrary units, models accounting for multiple scattering require reflectance values for input (e.g. the WAK model by Dymond et al. (2001)). For this reason, the image data were (in an approximation) radiometrically calibrated, i.e. converted to reflectance values.
The empirical line method was used (Smith and Milton, 1999). Reflectance values of reference plots were measured on the days of the image flights. Reference plots were selected for which Lambertian reflectance characteristics can be assumed, e.g. bright surfaces of concrete roads and dark surfaces of asphalt roads. The radiance values measured at these surfaces were converted to reflectance values by comparison (ratioing) with radiance values measured at a horizontal Spectralon reference panel of known reflectance. As the images used for this study were taken at different times, the differences in sun zenith angle at these times had to be taken into account. The following algorithm was used for this:

$$p_{iO} = p_i \frac{\cos\theta_{SO}}{\cos\theta_{Si}} = a + b\rho_i \qquad (1)$$

$$\rho = \frac{p\frac{\cos\theta_{SO}}{\cos\theta_S} - a}{b}$$

Here, p_i are the pixel values from the positions of the plots on the images and ρ_i are the corresponding reflectance values from the terrestrial spectroradiometric measurements. θ_{Si} is the zenith angle of the direction to the sun at the time the aerial photo showing the pixel value p_i was taken, and θ_{SO} is a standard value of the zenith angle of the sun used as a common reference: All pixel values of the plots for radiometric calibration, p_i, are converted to fictitious values p_{iO} they would have for this standard sun zenith angle. a and b are the coefficients of linear regression of the values p_{iO} to the values ρ_i. With this model, any pixel value p from an image taken at sun zenith angle θ_S can be converted to the reflectance value of the corresponding surface element assuming that it has Lambertian characteristics and that it was irradiated by the sun at the standard zenith angle. $\theta_{SO} = 30°$ was assumed for this work. This radiometric calibration procedure is approximative only, as it does not account for direction-dependent influences of the atmosphere. As a consequence, the BRDF functions obtained in this analysis include the direction-dependent influence of the atmosphere.
For BRDF analysis, sample plots of different forest types and, for comparison, of other land cover types were selected and located on all images on which they are recorded. Details on a selection of sample plots are presented in chapter 4. The view azimuth angle and the view zenith angle were calculated for the centre of each plot considering the location of the plot in the image (distance to image centre in x and y), the principal distance of the camera and the orientation angles ω, φ, and κ (roll, pitch and yaw) of the image. Finally, the mean of the pixel values was extracted for each plot, for each image on which the plot appears, and for each spectral band. These pixel values were converted to spectral reflectance values as described above.
The models listed in chapter 3 were fitted to the data and compared with regard to their suitability to estimate the model parameters from the relatively small number of directional

reflectance data and to predict the directional reflectance characteristics of the plots. The Levenberg–Marquardt optimization algorithm was used for retrieving the model parameters. The MPFIT package by Markwardt (2009) programmed in IDL (RSI, 2004) was applied. It allows placing constraints on parameter values and fixing parameters. The model parameters were partly restricted to physically meaningful values.

The models were evaluated using the coefficient of determination (R^2) and the symmetric mean absolute percentage error (sMAPE) that is defined as

$$sMAPE = \frac{1}{n-p}\sum_{i=1}^{n}\frac{|y_i - \hat{y}_i|}{(|y_i| - |\hat{y}_i|)/2}\cdot 100\% \quad , \quad (2)$$

where y_i is the measured reflectance, $\hat{y}_i$ is the modelled reflectance, n is the number of observations and p is the number of model parameters. The sMAPE was chosen instead of the RMSE, because it can be used to compare the error of sample plots that have different reflectance levels. The division by (n-p) instead of n incorporates model complexity in the error measure by penalizing a model for each model parameter.

3. BRDF MODELS

Over the past years, extensive efforts have been made to investigate the directional reflectance properties of surfaces. The result is a huge variety of models that predict the directional reflectance for all viewing geometries. The convention for denoting directions and angles is shown in Figure 2. The illumination and view directions are specified by 4 angles, the sun azimuth and zenith angle (ϕ_s and θ_s) as well as the view azimuth and zenith angle (ϕ_v and θ_v). The difference between the sun azimuth and the view azimuth angle is the relative azimuth ($\phi_r = \phi_s - \phi_v$).

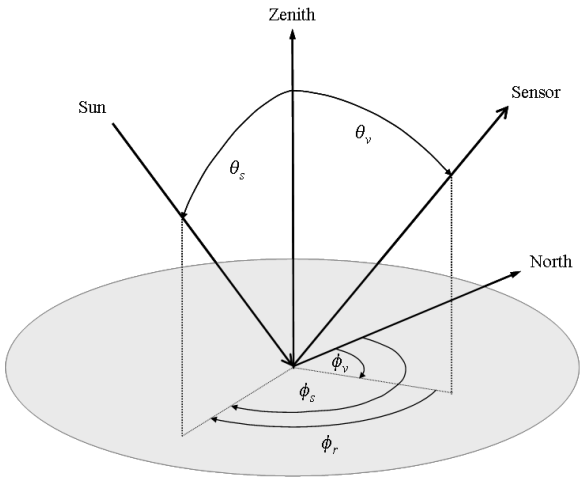

Figure 2. Convention for denoting directions and angles

The models employed in this study were selected according to the following criteria: physical, empirical and semi-empirical models should be included. The models should be suitable to describe the directional reflectance properties of vegetation in general and of forest canopies in particular and they should work for both visible and near-infrared light.

The following models were included in the comparison:

(1) Second-order polynomial (2DP): This model is a simple five-parameter second-order polynomial that is symmetric to the principal plane with two independent variables, the view zenith angle θ_v and the relative azimuth angle ϕ_r. The sun zenith angle θ_s is not considered.

(2) Walthall (WH): The Walthall model, derived by Walthall et al. (1985) and modified by Nilson and Kuusk (1989) to be reciprocal, is a purely empirical model for bare soil surfaces and vegetation canopy with four parameters. Liang and Strahler (1994) criticize that the model does not represent some important BRDF features such as the hot spot and amend the modified Walthall model by adding a hotspot component modelled by an exponential function with two additional parameters (WHL).

(3) Dymond (WAK): The model by Dymond et al. (2001) is a physical model that aims at reconstructing the bidirectional reflectance of homogeneous and closed vegetation canopies with randomly oriented leaves. Three parameters are used, one for the leaf reflectance and two to characterize the canopy phase function. The model is applicable to visible light and near-infrared light. It includes a term derived by Hapke (1981) to account for multiple scattering that is relevant in the near-infrared part of the spectrum. Two versions are proposed, WAK I and WAK II. The WAK II model rounds the hotspot as observed in the reflectance data of full size canopies, where there is both direct and diffuse illumination.

(4) Roujean (ROUJ): The model of Roujean et al. (1992) was the first kernel-driven model. It consists of a volume scattering kernel and a geometric-optical kernel. The volume scattering kernel is deduced from a formula by Ross (1981) and is suitable rather for optically thick than thin domains, i.e. for canopies with high values of leaf area index (LAI). Maignan et al. (2004) propose a modification of the volume scattering kernel to account for the hot spot more effectively (ROUJM). In contrast to the modification proposed by Chen and Cihlar (1997), no additional parameter is required.

(5) Ross-Thick/Li-Sparse (RTLS): This model combines the volume scattering kernel by Ross (Ross-Thick kernel) as described above with a geometric-optical kernel deduced from the model by Li and Strahler (1992), which considers the shadowing produced by randomly located trees with spheroid crowns on a Lambertian background. Wanner et al. (1995) deduced the Li-Sparse kernel, an approximation for sparse ensembles of such trees. Additionally to the three parameters usually used in kernel-driven models, there are two internal parameters describing the shape (oblate/round/prolate) and relative height of the tree crowns. The crown parameters in the best way describing the actual scene can be found by testing various sets of parameters. Both kernels, the Ross-Thick kernel and the Li-Sparse kernel, are implemented in AMBRALS, a modelling tool for the MODIS bidirectional reflectance and albedo products (Wanner et al., 1997).

(6) Rahman-Pinty-Verstraete (RPV): The RPV model (Rahman et al. 1993) is, in contrast to kernel-driven models, a multiplicative semi-empirical model. The base model uses three parameters (RPV3P). This model can be modified to a four-parameter model (RPV4P) that can improve modelled bidirectional reflectance values especially in the hotspot region when the hotspot effect is very pronounced. The RPV model is used for the processing of MISR surface products (surface BRF, albedo, LAI, FPAR) (Diner et al 2008).

4. DATA

The study is based on images taken with a Vexcel UltraCamD camera (Leberl et al., 2003). The multispectral bands without pansharpening were used. Parameters of the camera relevant for this study are listed in Table 3. The forward overlap was >80 % and the side overlap was 30 %.

Parameter	
FOV across track	37.5°
FOV along track	55°
Max. view zenith angle (diagonal)	31°
Pixel size (multispectral) at flying height of 3.900 m	75 cm
Radiometric resolution	12 bit

Table 3. Specifications of the UltraCamD digital aerial camera

The images were taken in the Rax-Schneeberg region in the south of Lower Austria in July 2006. For this study, six sample plots of different forest types and land cover types listed in Table 4 were selected. Criteria for the selection were moderate slope angles (<25 degree) and homogeneity in terms of tree species composition, development class and crown canopy closure. Furthermore, it was important that each plot is shown on images of two neighbouring flight lines to assure that the number of observations from different points of view is sufficient for the model fitting procedure. In Table 4, the area of each plot, the number of points of view and the range of the phase angle (i.e. the angle between the sun and view vector) is specified. The variation of the sun zenith angle is small for the entire image data set (27.1 to 30.7 degree), as the images were taken within a time interval of a few hours only.

SP		**Area [m²]**	**View directions**	**Phase angle**
1	Asphalt	130	16	8° - 48°
2	Grassland	160	13	16° - 57°
3	Young deciduous stand	350	12	5° - 38°
4	Old deciduous stand	700	11	5° - 50°
5	Young coniferous stand	650	10	6° - 52°
6	Old coniferous stand	2500	14	13° - 54°

Table 4. Sample plots

5. RESULTS

Due to limited space, only results for the near infrared band are given here.

As shown in Table 5, R^2 is quite high for all models and all sample plots. It lies between 0.852 (grassland, WAK I) and 0.999 (old coniferous stand, WHL). As R^2 is dependent on the variance of the observed values, here mainly caused by the direction-dependent reflectance, R^2 is generally lower for those sample plots that show smaller direction-dependent reflectance properties (asphalt, grassland). Thus, R^2 can only be compared for different models applied to the same sample plot. WHL achieves the highest R^2 for all sample plots but one (old deciduous stand), where WAK II outperforms the other models. However, it has to be considered that WHL is the model with the biggest number of model parameters (6). Obviously, the WHL model tends to overfitting due to the relatively small number of available observations (Table 4). Furthermore, the value of this purely empirical model is limited, because the model parameters cannot be applied to conditions (e.g. illumination geometry) that are outside the range covered by the observations, and because it does not permit the retrieval of biophysical parameters (e.g. LAI).

In contrast to R^2, the symmetric mean absolute percentage error (sMAPE; Equation 2) takes into account the model complexity, i.e. the number of parameters (Figure 8). However, it has to be noted that the different number of observations per sample plot still affects the comparison of different sample plots based on this measure.

The errors for the most successful models were between 3 and 6 %. The poorest results were achieved for SP5 (old coniferous stand).

For two sample plots (old coniferous stand, young coniferous stand) the difference in R^2 and sMAPE between ROUJ and ROUJM as well as between RPV3P and RPV4P is clearly visible. The hotspot effect is very pronounced for these test sites and it can be concluded that the hotspot-modification of these models is very effective. On the other hand, there is hardly any difference between RTLS and RTLSM, sMAPE is low for both models. The performance of ROUJ and RTLS, both kernel-driven models that apply the same volume scattering kernel, differs significantly. This indicates that the geometric-optical kernel of RTLS outperforms that of ROUJ, which is probably achieved by incorporating the two crown parameters. The simple second-order polynomial model performs surprisingly well except for the two sample plots with pronounced hotspot effect (young coniferous stand, old coniferous stand).

Figure 6 and 7 show examples for the BRDF (or, to be more specific, approximations to the BRDF, as noted above) at constant sun zenith angle for SP5 and SP6 modelled with the 3-parameter RPV model (RPV3P). The observations used to retrieve the model parameters are plotted (empty squares) and connected with the modelled values (filled squares) by a vertical line. The BRDF of the young coniferous stand is bowl-shaped with a slightly-developed hotspot effect, whereas the BRDF of the old coniferous stand is more bell-shaped and shows a pronounced increase of reflectance in the hotspot region. The reflectance modelled for the old coniferous stand is significantly lower than that of the young coniferous stand (apart from the hotspot region) which may be due to shadows.

The model parameters of the semi-empirical and physical models in most cases were plausible and touched the pre-set boundaries only in a few cases. Problems emerged if observations close to the hotspot were missing.

Model	**SP1** asphalt	**SP2** grass	**SP3** y dec	**SP4** old dec	**SP5** y con	**SP6** old con
2DP	0.914	0.856	0.938	0.990	0.958	0.975
WH	0.870	0.905	0.958	0.976	0.980	0.960
WHL	0.919	0.919	0.980	0.986	0.994	0.999
WAK I	0.903	0.852	0.965	0.989	0.975	0.995
WAK II	0.907	0.869	0.966	0.993	0.955	0.972
ROUJ	0.882	0.861	0.926	0.978	0.908	0.888
ROUJM	0.893	0.860	0.924	0.982	0.970	0.960
RTLS	0.897	0.870	0.927	0.985	0.989	0.997
RTLSM	0.893	0.867	0.927	0.983	0.989	0.998
RPV3P	0.909	0.857	0.921	0.981	0.944	0.968
RPV4P	0.909	0.858	0.927	0.985	0.980	0.998

Table 5. Coefficient of determination (R^2)

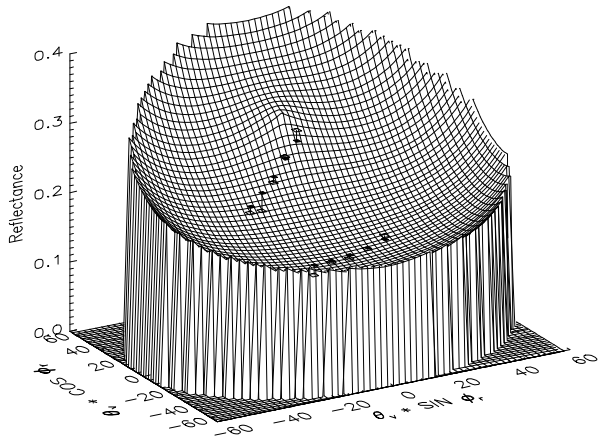

Figure 6. BRDF modelled with the 3-parameter RPV model (RPV3P) for a young coniferous stand (SP5), $\theta_s = 30^o$

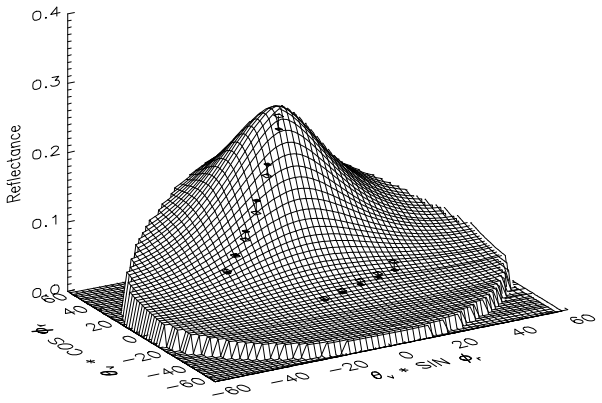

Figure 7. BRDF modelled with the 3-parameter RPV model (RPV3P) for an old coniferous stand (SP6), $\theta_s = 30^o$

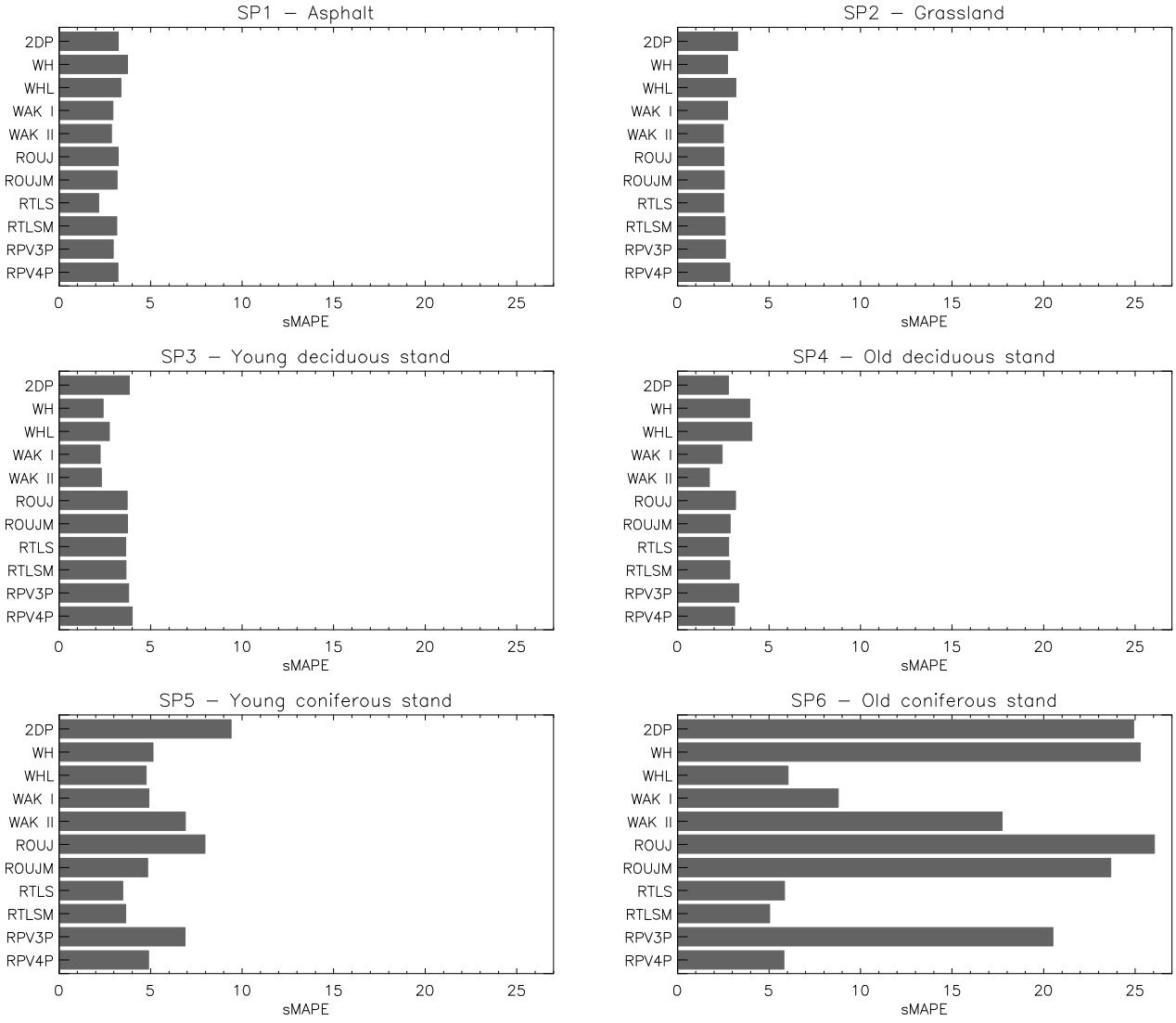

Figure 8. Symmetric mean absolute percentage error (sMAPE) for different BRDF-models and different land cover and forest types (SP1-SP6)

6. CONCLUSIONS

It has been shown that the parameters of BRDF models describing individual forest plots can be estimated from digital aerial photos taken with a frame camera with large forward and side overlap. The obtained results are plausible. Differences in the performance of the models for different forest plots can be explained taking into account the special assumptions on which the models are based and the special properties of the observed forest stands.

The following improvements and extensions are to be considered in future work:

(1) The number of test plots in the current study is small. More plots will be evaluated in order to deduce information on the variation of the derived model parameters for test plots of identical forest types, to assess the potential of BRDF characteristics obtained from aerial photos for discriminating forest types and determining forest parameters, and to verify this with independent test plots.

(2) The performance of the models in describing the dependence of the BRDF on the sun zenith angle will be studied using data sets with a higher variation of this parameter.

(3) The radiometric calibration will be improved by accounting for the non-Lambertian characteristics of the sample plots and the direction-dependent influence of the atmosphere.

(4) The analysis will be extended to pixel windows of different sizes down to full resolution provided by the camera (single pixels), in order to obtain more insight into the functioning and the performance of the models.

REFERENCES

Chen, J. M., Cihlar, J., 1997. A hotspot function in a simple bidirectional reflectance model for satellite applications. *Journal of Geophysical Research*, 102 (D22), pp. 25907-25913.

Diner, D. J., Martonchik, J. V., Borel, Ch., Gerstl, S. A. W., Gordon, H. R., Knyazikhin, Y., Myneni, R., Pinty, B. and Verstraete, M. M., 2008. Multi-angle Imaging Spectro-Radiometer - Level 2 Surface Retrieval Algorithm Theoretical Basis, Revision E. Jet Propulsion Laboratory, California Institute of Technology. http://www-misr.jpl.nasa.gov (accessed 25 Oct. 2009)

Dymond, J. R., Shepherd, J. D., Qi, J., 2001. A simple physical model of vegetation reflectance for standardising optical satellite imagery. *Remote Sensing of Environment*, 77 (2), pp. 230-239.

Dymond, J. R., Trotter, C. M., 1997. Directional reflectance of vegetation measured by a calibrated digital camera. *Applied Optics*. 36 (18), pp. 4314-4319.

Hapke, B., 1981. Bidirectional reflectance spectroscopy, 1. Theory. *Journal of Geophysical Research*, 86, pp. 3039-3054.

Leberl, F., Perko, R., Gruber, M., Ponticelli, M., 2003. The UltraCam large format aerial digital camera system. *Proceedings of the American Society for Photogrammetry and Remote Sensing Annual Convention*, Anchorage, Alaska, 5-9 May 2003, published on CD, no page numbering.

Li, X., Strahler, A. H., 1992. Geometric-Optical Bidirectional Reflectance Modeling of the discrete crown vegetation canopy: effect of crown shape and mutual shadowing. *IEEE Transactions on Geoscience and Remote Sensing*, 30 (2), pp. 276-292.

Liang, S., Strahler, A. H., 1994. Retrieval of surface BRDF from multiangle remotely sensed data. *Remote Sensing of Environment*, 50, pp. 18-30.

Maignan, F., Bréon, F. M., Lacaze, R., 2004. Bidirectional reflectance of Earth targets: evaluation of analytical models using a large set of spaceborne measurements with emphasis on the hot spot. *Remote Sensing of Environment*, 90 (2), pp. 210-220.

Markwardt, C. B., 2009. Non-linear least squares fitting in IDL with MPFIT. In: Bohlender, D. A., Durand, D., Dowler, P. (eds.), *Proceedings of Astronomical Data Analysis Software and Systems XVIII*, Quebec, Canada, ASP Conference Series, Vol. 411, Astronomical Society of the Pacific: San Francisco, pp. 251-254.

Nilson, T., Kuusk, A., 1989. A reflectance model for the homogeneous plant canopy and its inversion. *Remote Sensing of Environment*, 27, pp 157-167.

Rahman, H., Pinty, B., Verstraete, M. M., 1993. Coupled surface-atmosphere reflectance (CSAR) model - 2: Semiempirical surface model usable with NOAA advanced very high resolution radiometer data," *Journal of Geophysical Research*, 98, pp. 20791–20801.

Ross, J., 1981. *The radiation regime and architecture of plant stands*. Dr. W. Junk Publishers. The Hague.

Roujean, J.-L., Leroy, M., Deschamps, P.-Y., 1992. A bidirectional reflectance model of the earth's surface for the correction of remote sensing data. *Journal of Geophysical Research*, 97 (D18), pp. 20455-20468.

RSI, 2004. IDL – Interactive Data Language. Boulder, CO

Schaepman-Strub, G., Schaepman, M. E, Painter, T. H., Dangel, S., Martonchik, J. V., 2006. Reflectance quantities in optical remote sensing – definitions and case studies. *Remote Sensing of Environment*, 103, pp. 27-42.

Smith, G. M., Milton, E. J., 1999. The use of the empirical line method to calibrate remotely sensed data to reflectance. *Int. Journal of Remote Sensing*, 20 (13), pp. 2653-2662.

Walthall, C. L., Norman, J. M., Welles, J. M., Campbell, G., Blad, B. L. 1985. Simple equation to approximate the bi-directional reflectance from vegetation canopies and bare soil surfaces. *Applied Optics*, 24, pp. 383-387.

Wanner, W., Li, X., Strahler, A. H. 1995. On the derivation of kernels for kernel-driven models of bidirectional reflectance. *Journal of Geophysical Research*, 100 (D10), pp. 21077-21089.

Wanner, W., Strahler, A. H., Hu, B., Lewis, P., Muller, J.-P., Li, X., Schaaf, C. L. B., Barnsley, M. J. (1997). Gobal retrieval of bidirectional reflectance and albedo over land from EOS MODIS and MISR data: Theory and algorithm. *Journal of Geophysical Research*, 102 (17), pp. 17143-17161.